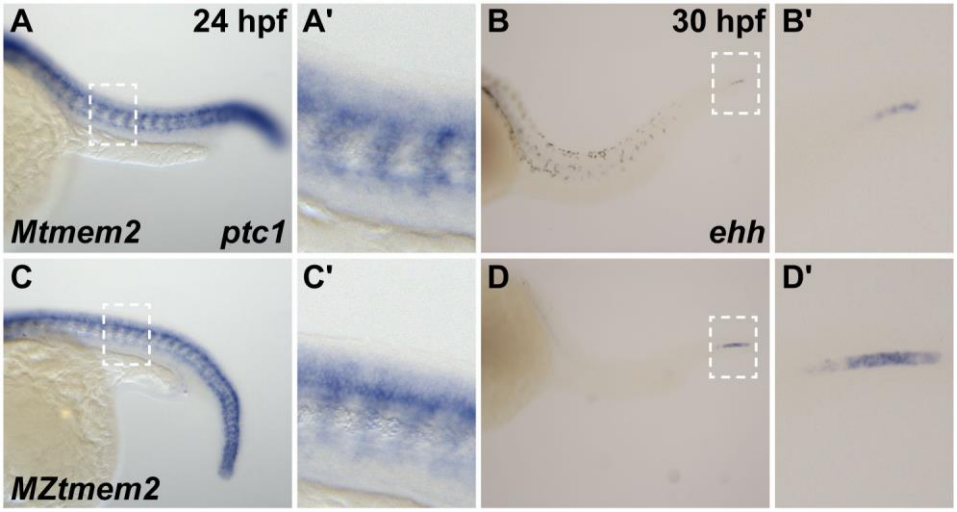

Fig. S1. Hedgehog signaling and notochord differentiation are intact in *MZtmem2* mutants. (**A-D**) In situ hybridization depicts expression of *ptc1* at 24 hpf (A,C) or *ehh* at 30 hpf (B,D) in *Mtmem2* (A,B) and *MZtmem2* (C,D) siblings, lateral views, anterior at left. A'-D' show closer views of regions outlined by white rectangles in A-D. (A,C) Expression of *ptc1* serves as a reporter of Hedgehog signaling. Loss of Hedgehog signaling causes formation of U-shaped somites (Lewis et al., 1999; Schauerte et al., 1998; van Eeden et al., 1996), but Hedgehog signal transduction seems relatively robust in *MZtmem2* mutants. (B,D) Notochord maturation is accompanied by loss of expression of *ehh*, a chordamesoderm marker (Parsons et al., 2002; Stemple, 2005). As notochord differentiation proceeds from anterior to posterior, *ehh* is visible only at the caudal end of the notochord by 30 hpf (B). The progression of differentiation is relatively normal in *MZtmem2* mutants (D), although the slightly increased extent of *ehh* expression that remains at 30 hpf suggests a slight delay.

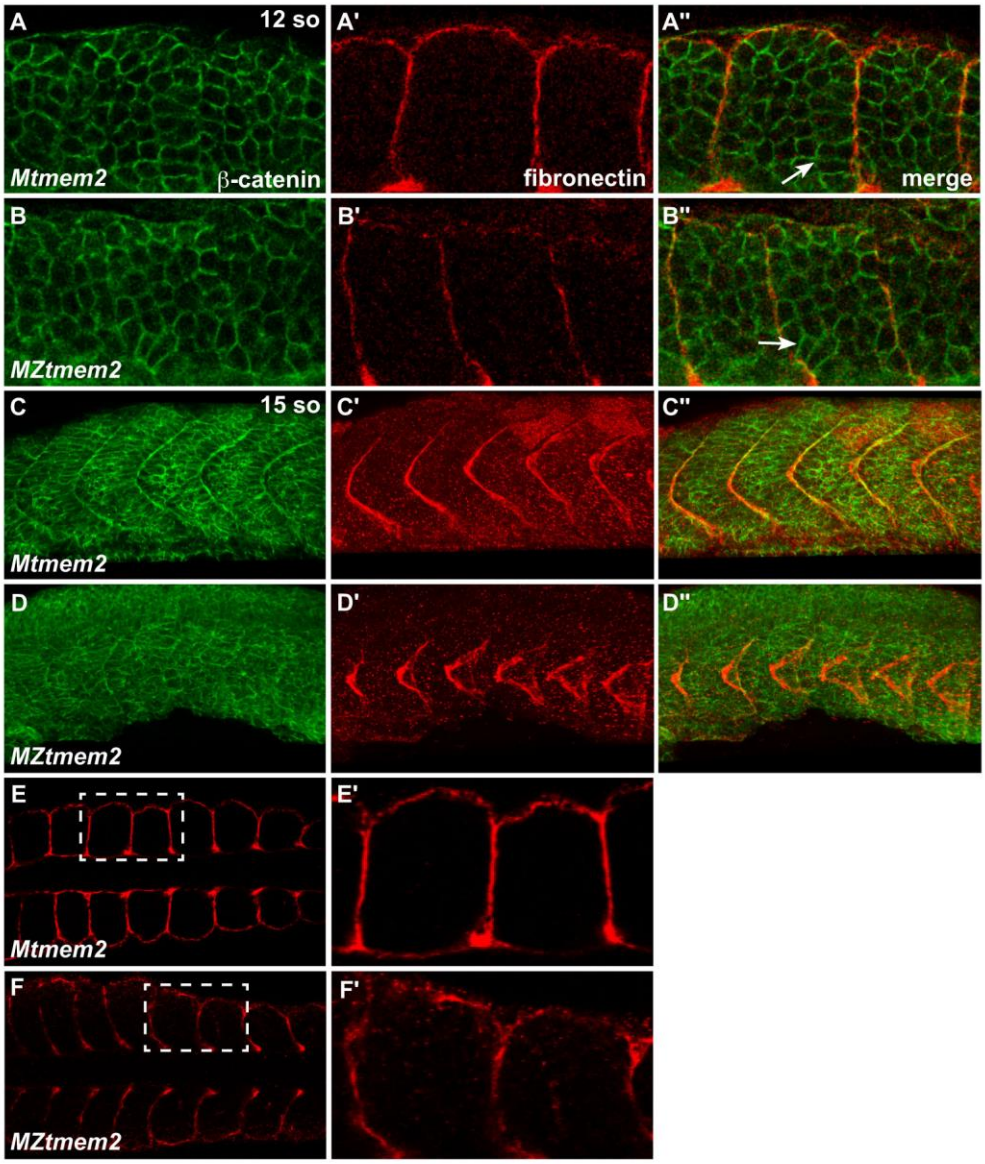

Fig. S2. Initial formation of somite borders appears normal in *MZtmem2* mutants. (**A-F**) Immunofluorescence indicates localization of fibronectin (red) relative to β-catenin (green) at 12 so (A-B) and 15 so (C-F). (A-B) Dorsal views, anterior to the left, of the right myotome show fibronectin localization at somite boundaries. In *MZtmem2* mutants (B'), fibronectin is deposited at each somite boundary, in a pattern comparable to that seen in *Mtmem2* siblings (A'). Additionally, muscle precursor cells at the borders of *MZtmem2* somites exhibit characteristic elongation indicative of the formation of epithelial somite boundaries (Henry et al., 2005) (B'', arrow), just as in *Mtmem2* siblings (A'', arrow). These results suggest that the initial formation of somite boundaries proceeds normally in *MZtmem2* mutants. (C-D) Lateral views, dorsal up, display

fibronectin localization at somite boundaries at 15 so, when the earliest aberrations in fibronectin organization appear in *MZtmem2* mutants. In *MZtmem2* mutants (D'), fibronectin is present at somite boundaries, but seems disorganized, in contrast to the sharply defined fibronectin deposition present in *Mtmem2* siblings (C'). (E-F) Dorsal views, anterior to the left, indicate that fibronectin is present at somite boundaries at 15 so in *MZtmem2* mutants (F), as it is in *Mtmem2* siblings (E). E' and F' show closer views of regions outlined by white rectangles in E and F.

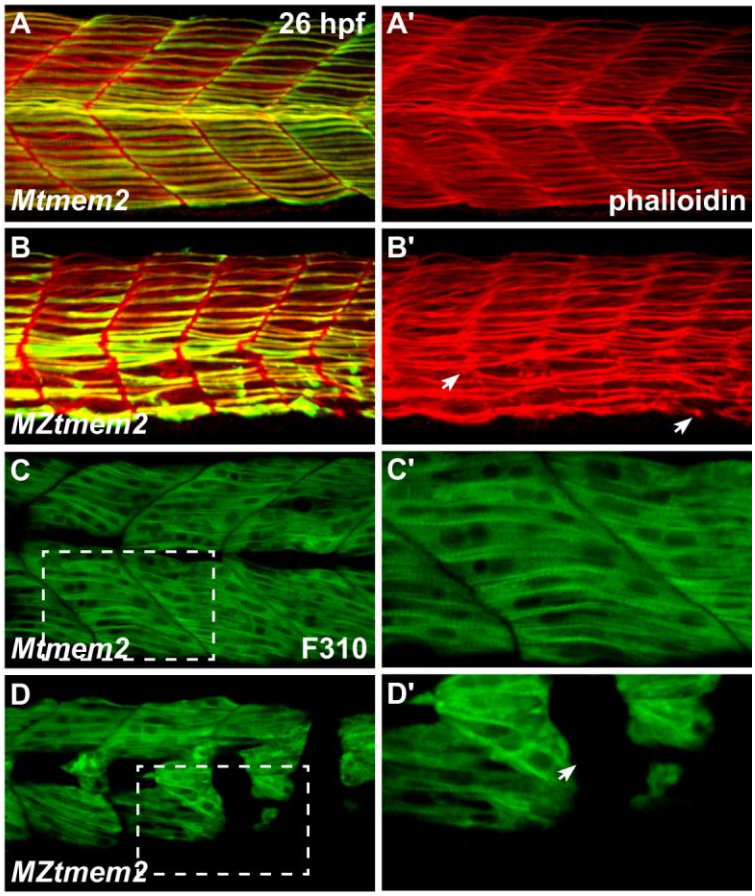

Fig. S3. Disruption of fast muscle fiber attachment in *MZtmem2* mutants. (**A-D**) Immunofluorescence reveals muscle fiber organization, using phalloidin (red in A,B) to recognize both fast and slow fibers, F59 (green in A,B) to recognize slow fibers (Devoto et al., 1996), and F310 (green in C,D) to recognize fast fibers (Nord et al., 2014); lateral views, dorsal up, at 26 hpf. (A,B) In addition to exhibiting detachment of $F59^{+}$ slow muscle fibers (B); see also Fig. 1H), *MZtmem2* mutants display detachment of $F59^{-}$ fast muscle fibers (arrows, B'), in contrast to the attached fibers observed in *Mtmem2* siblings (A). (C,D) Similarly, *MZtmem2* mutants (D) display detachment of $F310^{+}$ fast muscle fibers (arrow, D2), in contrast to the attachment seen in *Mtmem2* siblings (C). C' and D' show closer views of regions outlined by white rectangles in C and D.

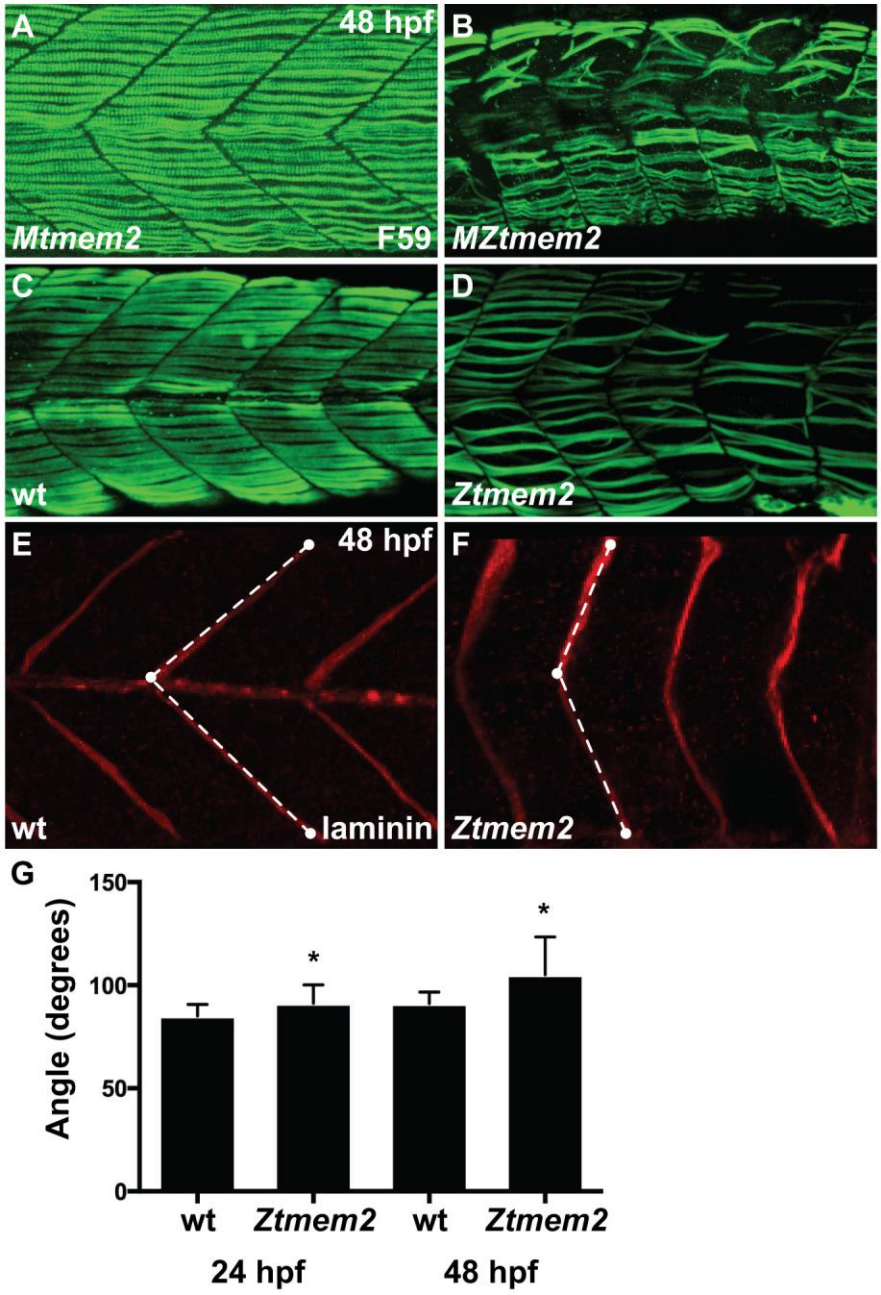

Fig. S4. Impairment of muscle fiber organization in zygotic *tmem2* mutants. (**A-D**) Immunofluorescence with F59 (green) reveals slow muscle fiber organization; lateral views with dorsal up at 48 hpf. At this stage, *MZtmem2* mutants (B) exhibit detachment and disorganization of slow muscle fibers, in contrast to the normal attachment seen in their *Mtmem2* siblings (A). Although we have not observed muscle fiber detachment in zygotic *tmem2* (*Ztmem2*) mutants at 24 hpf (data not shown), we have found fiber detachment and disorganization in some *Ztmem2* mutants (D) by 48 hpf (n=4 out of 33

Ztmem2 mutants examined). (**E,F**) Immunofluorescence detecting laminin (red) deposition at the MTJ reveals somite shape defects in *Ztmem2* mutants. In wild-type (E) and *Ztmem2* (F) sibling embryos, somite shape was evaluated by measuring the angle formed at the MTJ. White dots represent examples of the reference points chosen at the horizontal myoseptum, the dorsal edge of the MTJ, and the ventral edge of the MTJ; dashed lines represent the angle measured using ImageJ software. (**G**) Bar graph compares average angles formed at the MTJ in wild-type and *Ztmem2* embryos at 24 hpf and 48 hpf (in wild-type, n=85 at 24 hpf and n=75 at 48 hpf; in *Ztmem2*, n=52 at 24 hpf and n=154 at 48 hpf). Error bars indicate s.d., and asterisks indicate a significant difference from wild-type (Student's t-test; $p<0.0001$). Somite shapes in *Ztmem2* mutants become less chevron-shaped and more U-shaped over time, presumably as maternal supplies of *tmem2* are depleted and muscle fiber defects accumulate.

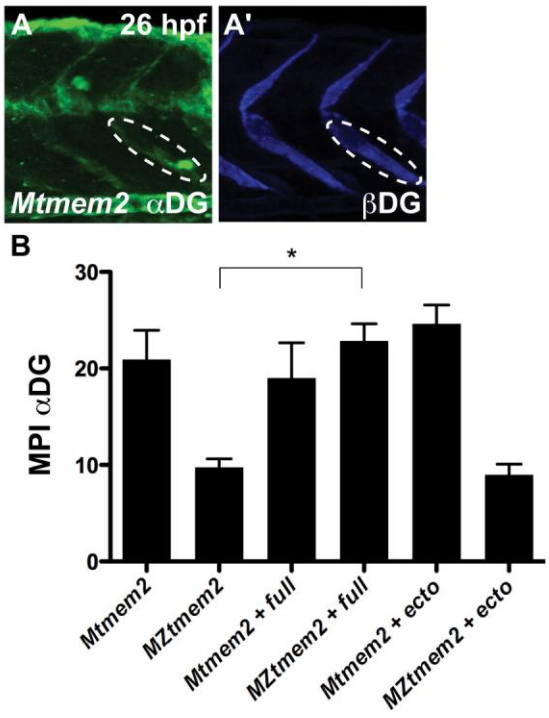

Fig. S5. Quantification of intensity of immunostaining for dystroglycan at the MTJ. (**A)** Confocal reconstruction depicts immunostaining for glycosylated αDG (A) and βDG (A') in a *Mtmem2* embryo at 26 hpf; lateral view, dorsal up. To quantify the intensity of immunostaining through the entire depth of the confocal stack, we used Imaris software to rotate each reconstruction 30 degrees toward the right and then used ImageJ software to measure the mean pixel intensity (MPI) within an oval-shaped region of interest positioned at the MTJ. Ovals of the same size and in the same position were used to measure MPI for both glycosylated αDG and βDG (as outlined in A and A'). (**B**) Bar graph compares MPI of immunostaining for glycosylated αDG at the MTJ at 26 hpf; error bars indicate s.e.m. For each condition, we measured the MPI at 5 different MTJs in each of 3 representative embryos (*Mtmem2*: 2 embryos presenting normal staining and 1 embryo presenting traces of staining; *MZtmem2*: 2 embryos presenting traces of staining and 1 embryo presenting no staining; *Mtmem2* + full: 2 embryos presenting normal staining and 1 embryo presenting traces of staining; *MZtmem2* + full: 3 embryos presenting normal staining; *Mtmem2* + ecto: 3 embryos presenting normal staining; *MZtmem2* + ecto: 2 embryos presenting traces of staining and 1 embryo presenting no staining). Introduction of full-length Tmem2, but not the Tmem2 ectodomain, caused evident improvement in αDG glycosylation in *MZtmem2* mutants. Asterisk indicates significant difference from *MZtmem2* (Student's t-test; $p<0.01$). See also Fig. 4H and Table S3.

SUPPLEMENTAL REFERENCES

Devoto, S. H., Melancon, E., Eisen, J. S. and Westerfield, M. (1996). Identification of separate slow and fast muscle precursor cells in vivo, prior to somite formation. *Development* **122**, 3371-3380.

Henry, C. A., McNulty, I. M., Durst, W. A., Munchel, S. E. and Amacher, S. L. (2005). Interactions between muscle fibers and segment boundaries in zebrafish. *Dev. Biol.* **287**, 346-360.

Lewis, K. E., Currie, P. D., Roy, S., Schauerte, H., Haffter, P. and Ingham, P. W. (1999). Control of muscle cell-type specification in the zebrafish embryo by Hedgehog signalling. *Dev. Biol.* **216**, 469-480.

Nord, H., Burguiere, A. C., Muck, J., Nord, C., Ahlgren, U. and von Hofsten, J. (2014). Differential regulation of myosin heavy chains defines new muscle domains in zebrafish. *Mol. Biol. Cell* **25**, 1384-1395.

Parsons, M. J., Pollard, S. M., Saude, L., Feldman, B., Coutinho, P., Hirst, E. M. and Stemple, D. L. (2002). Zebrafish mutants identify an essential role for laminins in notochord formation. *Development* **129**, 3137-3146.

Schauerte, H. E., van Eeden, F. J., Fricke, C., Odenthal, J., Strahle, U. and Haffter, P. (1998). Sonic hedgehog is not required for the induction of medial floor plate cells in the zebrafish. *Development* **125**, 2983-2993.

Stemple, D. L. (2005). Structure and function of the notochord: an essential organ for chordate development. *Development* **132**, 2503-2512.

van Eeden, F. J., Granato, M., Schach, U., Brand, M., Furutani-Seiki, M., Haffter, P., Hammerschmidt, M., Heisenberg, C. P., Jiang, Y. J., Kane, D. A., et al. (1996). Mutations affecting somite formation and patterning in the zebrafish, Danio rerio. *Development* **123**, 153-164.

Table S1. Rescue of muscle fiber attachment by injection of *tmem2* mRNA.

		Muscle fiber phenotype at 48 hpf		
		many detached	few detached	all attached
Mtmem2	uninjected			8/8 (100%)
MZtmem2	uninjected	9/9 (100%)		
Mtmem2	full-length			7/7 (100%)
MZtmem2	full-length	1/17 (6%)	1/17 (6%)	15/17 (88%)
Mtmem2	ectodomain		1/2 (50%)	1/2 (50%)
MZtmem2	ectodomain	2/8 (25%)	3/8 (25%)	3/8 (37.5%)

Summary of 3 independent experiments evaluating whether injection of mRNA encoding either full-length Tmem2 or the Tmem2 ectodomain can rescue the muscle fiber detachment defects in *MZtmem2* mutants. Genotype (*Mtmem2* and *MZtmem2*) and mRNA injected (uninjected, full-length, or ectodomain) are provided for each set of embryos. Data indicate the fraction of examined embryos displaying severe muscle fiber detachment, a small number of detached fibers, or normal fiber attachment. For each embryo, we examined 11 somites on the left side of the myotome, using immunofluorescence with F59 and phalloidin to reveal muscle fiber organization. Embryos were classified as "many detached" if fiber detachment was evident in all 11 somites examined and as "few detached" if fiber detachment was evident in 5 or fewer somites. In a subset of these embryos, we counted the numbers of attached and detached $F59^{+}$ fibers within the 11 somites examined, and this quantification is presented in Fig. 1L. Full-length Tmem2 and the Tmem2 ectodomain are both capable of rescuing muscle fiber attachment in *MZtmem2* mutants, although full-length Tmem2 seems to rescue more efficiently.

Table S2. Rescue of cardiac fusion by injection of *tmem2* mRNA.

		Cardiac fusion phenotype at 24 hpf			
		cardia bifida	partial fusion	cardiac ring	heart tube
Mtmem2	uninjected				8/8 (100%)
MZtmem2	uninjected	19/23 (83%)	4/23 (17%)		
Mtmem2	full-length				27/27 (100%)
MZtmem2	full-length			4/18 (22%)	14/18 (78%)
Mtmem2	ectodomain		1/13 (8%)		12/13 (92%)
MZtmem2	ectodomain	2/28 (7%)	7/28 (25%)	17/28 (61%)	2/28 (7%)

Summary of 4 independent experiments evaluating whether injection of mRNA encoding either full-length Tmem2 or the Tmem2 ectodomain can rescue the cardiac fusion defects in *MZtmem2* mutants. Genotype (*Mtmem2* and *MZtmem2*) and mRNA injected (uninjected, full-length, or ectodomain) are provided for each set of embryos. Cardiac phenotypes were assessed through in situ hybridization for *myl7*, as in Fig. 3F-K. Data indicate the fraction of examined embryos displaying cardia bifida (as in Fig. 3G), partial fusion at the posterior end of the cardiac primordia (as in Fig. 3H), fusion to form a ring of cardiomyocytes (as in Fig. 3K), or normal heart tube assembly (as in Fig. 3J). Full-length Tmem2 and the Tmem2 ectodomain are both capable of rescuing cardiac fusion in *MZtmem2* mutants, although full-length Tmem2 seems to rescue more efficiently.

Table S3. Rescue of αDG glycosylation by injection of *tmem2* mRNA.

		IIH6 staining at 26 hpf		
		no staining	traces of staining	normal staining
Mtmem2	uninjected		4/26 (15%)	22/26 (85%)
MZtmem2	uninjected	18/32 (56%)	14/32 (44%)	
Mtmem2	full-length		1/9 (11%)	8/9 (89%)
MZtmem2	full-length		2/13 (15%)	11/13 (85%)
Mtmem2	ectodomain			5/5 (100%)
MZtmem2	ectodomain	1/7 (14%)	6/7 (86%)	

Summary of 3 independent experiments evaluating whether injection of mRNA encoding either full-length Tmem2 or the Tmem2 ectodomain can rescue αDG glycosylation at the MTJ in *MZtmem2* mutants. Genotype (*Mtmem2* and *MZtmem2*) and mRNA injected (uninjected, full-length, or ectodomain) are provided for each set of embryos. αDG glycosylation was assessed through immunostaining with the antibody IIH6, as in Fig. 4E'-G'. Data indicate the fraction of examined embryos displaying no IIH6 staining at the MTJ, trace amounts of IIH6 staining at the MTJ (as in Fig. 4F'), or normal IIH6 staining at the MTJ (as in Fig. 4E' and 4G'). In a subset of these embryos, we measured the intensity of IIH6 staining at 5 different MTJs in each of 3 representative embryos; the results of this quantitative analysis are presented in Figs. 4H and S5. Full-length Tmem2 is capable of rescuing αDG glycosylation at the MTJ in *MZtmem2* mutants, whereas introduction of the Tmem2 ectodomain is not sufficient to rescue normal levels of glycosylated αDG in this context.

Table S4. Antibodies used for immunofluorescence.

	Antigen	Reagent	Vendor	Dilution
Primary antibodies	Myosin heavy chain	Mouse monoclonal (F59)	Developmental Studies Hybridoma Bank (supernatant)	1:10
	Laminin	Rabbit polyclonal	Sigma (#L9393)	1:100
	Fibronectin	Rabbit polyclonal	Sigma (#F3648)	1:100
	β-catenin	Mouse monoclonal (15B8)	Sigma (#C7207)	1:500
	Tropomyosin	Mouse monoclonal (CH1)	Developmental Studies Hybridoma Bank (supernatant)	1:10
	Paxillin	Mouse monoclonal (349)	BD Biosciences (#612405)	1:50
	FAK [pY^{397}]	Rabbit polyclonal	Invitrogen (#44-624G)	1:50
	Myosin heavy chain	Mouse monoclonal (F310)	Developmental Studies Hybridoma Bank (supernatant)	1:10
	α-dystroglycan	Mouse monoclonal (IIH6-C4)	Santa Cruz Biotechnology (#sc-73586)	1:50
	β-dystroglycan	Mouse monoclonal (43DAG1/8D5)	Novocastra (#NCL-b-DG)	1:50
Secondary antibodies	Rabbit IgG	Goat polyclonal; Alexa Fluor 594	Molecular Probes (#A11012)	1:200
	Rabbit IgG	Goat polyclonal; Alexa Fluor 647	Molecular Probes (#A21245)	1:200
	Mouse IgG1	Goat polyclonal; FITC	Southern Biotechnology (#1070-02)	1:100